Colloid Polym Sci 279:153–160 (2001)

ORIGINAL CONTRIBUTION

P. H. F. Hansen
T. Arnebrant
L. Bergström

Shear induced aggregation of a pectin stabilised emulsion in two dimensions

Received: 7 June 2000
Accepted: 1 August 2000

P. H. F. Hansen (✉) · T. Arnebrant
L. Bergström
Institute for Surface Chemistry
YKI, P.O. Box 5607
S-114 86 Stockholm, Sweden
e-mail: peter.hansen@surfchem.kth.se

Abstract Shear induced aggregation of a Pectin stabilised emulsion trapped at the air-liquid interface was studied in a Couette system by video enhanced microscopy. From dimension analysis, Brownian motion was identified to enhance the probability of bond formation. The characteristic time scale of aggregation was found to scale as $t_c \sim \eta/\phi$ rather than $t_c \sim 1/\dot{\gamma}\phi$ as expected for orthokinetic aggregation. The structure of very large clusters showed strongly rearranged strands and fractal scaling for low $\dot{\gamma}$ and ϕ, analysed by density autocorrelation. At high $\dot{\gamma}$ and ϕ, the cluster was dominated by larger drops and no fractal scaling could be determined for the accessible length scales.

Key words Colloidal aggregation · Two dimensions · Pectin · Kinetics · Emulsion · Cluster structure · Fractal

Introduction

Aggregation of colloid systems has received much attention because of its technical importance, e.g. as food emulsions and cosmetics. The theoretical foundation of how particle interactions affect the aggregation kinetics and the final cluster structure has been obtained from model experiments and computer simulations [1, 2]. The models have mainly dealt with monodisperse particle systems and concerned rigid particles. Only recently, investigations have begun by computer simulation of Brownian aggregation of slightly polydisperse system [3], and for bi- and tri-dispersed systems [4]. It was shown that the polydispersity does not change the fractal scaling of the aggregates, but affects the structure at short length scales, comparable to the mean particle size [3, 4].

In shear induced aggregation, the collision frequency scales with the object size and is not compensated for by larger diffusion of the smaller objects. When only convection is considered for highly attractive monodisperse particles, both simulations [5] and experiments [6] show that the aggregation rate is increased by a predominance of cluster-cluster aggregation. Differences in structure, compared to a diffusion-controlled system, occur when the particle bonds are weakened to allow rearrangement and breakup [7]. If the particles are affected by both diffusion and convection, the aggregation process display a transition from particle-cluster to cluster-cluster aggregation when the average cluster size increases. This has been demonstrated experimentally in both two [8] and three [9] dimensions.

In this context, a polydisperse system is expected to display a complex behaviour as the relative importance of diffusion and particle rearrangements vary with the particle size. Recently, Wilson et al. [10] numerically investigated the combination of diffusion and convection for a weakly interacting system, including double-layer repulsion. They found that, although diffusion or convection alone were unable to aggregate the system, the combination of the two caused significant aggregation. Consequently, in a polydisperse emulsion, where a large region in parameter space is covered simultaneously, suitable combinations of drop sizes may be favoured in the aggregation process.

Experimental studies using polydisperse particles are scarce. This is probably related to the difficulty in evaluating the data, using, e.g. light scattering where the

form and structure factor has to be separated. This is a procedure that becomes difficult when both a size distribution of primary particles and a size distribution of aggregates are present and spatially distributed [11]. In this work, we chose to simplify the experimental conditions by investigating a two-dimensional system of emulsion drops trapped at the air-liquid interface. Thereby, the structure and the aggregation kinetics may be monitored by ordinary light microscopy, and we can use customised image analysis to determine the spatial distribution of drops in the clusters.

We have chosen to investigate an oil-in-water emulsion stabilised by pectin (mainly polygalacturonic acid with varying amounts of methoxylated carboxylic acid groups depending on preparation). The use of pectin is growing in consumer products based on natural ingredients, e.g. in cosmetics [12]. Pectin additions result in emulsions that are stable over a wide pH-range [13]. The emulsions showed limited coalescence and no flocculation in the absence of $CaCl_2$.

Initial experiments, carried out using sodium caseinate and β-casein stabilised emulsions, had the drops trapped within a viscoelastic surface film of the emulsifier. These latter observations are in line with the pronounced viscoelasticities reported for interfacial layers of proteins of both globular and flexible types; see for example work by Graham and Phillips [14, 15], Dickinson et al. [16] and Murray et al. [17]. However, pectin was found to perform well in this respect, in agreement with the lower surface viscosities and elasticities reported [18].

This paper presents experimental results on how changes in electrolyte concentration, shear rate and surface fraction of emulsion influences the kinetics and the structure of the aggregates.

Materials and methods

The emulsion

The stock emulsion was prepared from rapeseed oil (Karlshamns, Sweden), consisting of 10% oil and 89% Milli-Q water which contained 1% (w/v) of pectin (high methoxyl citrus pectin, degree of esterification 68–75%, Classic CU 201, Herbstreith & Fox, Neuenburg, Germany). A log-normal volume-weighed diameter distribution, ranging from 0.05 μm to 40 μm was obtained by mixing 100 g solution in an Ultra-Turrax at 24,000 rpm for 60 s followed by treatment in a Microfluidizer for 60 s at a pressure of 5 bar. After preparation, the emulsion drops had a number volume mean diameter of 2.3 μm. The emulsion proved to be very stable; during 15 weeks of storage, the drop size distribution was only slightly shifted to a mean value of 3.6 μm.

Preparing the colloidal system

The stock emulsion was diluted to a volume fraction of 0.5% of oil. A total of 120 μl emulsion – divided into 20 drops – were spread at the air-liquid interface of a glycerol/water mixture (50/50 w/w). This resulted in thin surface films (20 μm thick) containing emulsion droplets that within 30 min were reduced to a monolayer at the interface when the less dense emulsion droplets creamed. Consequently, the drops became trapped at the air-liquid interface and formed a two-dimensional colloidal system of droplets partly immersed into the liquid. The fraction of surface covered by droplets, ϕ, were controlled by the initial amount of added emulsion and resulted in a value of $\phi \approx 0.1$ under the experimental conditions mentioned above.

Finally, interactions were modified by means of electrolyte concentration. After creation of the interfacial emulsion film, a volume of glycerol/water containing 0.91 mol/l $CaCl_2$ were added from the bottom of the cell to control the final bulk electrolyte concentration. In present work, the final concentration was set to 0.1, 0.3 or 0.5 mol/l $CaCl_2$ in the bulk solution. All glycerol/water mixtures were buffered with 50 mmol/l TRIS yielding a pH of 8.4.

The shear cell

Ordinary light microscopy and a specially made cell enabled the study of shear induced aggregation in two dimensions. The cell is basically a sealed container with two axis-symmetric cylinders that allows inspection by a microscope. This cell and the setup are described in detail elsewhere [8]. The gap between the cylinders, that rotate in opposite directions, is fairly wide (10.3 mm) to allow proper illumination of the interfacial emulsion by the microscope. The viscosity of the liquid in the cell had to be increased to 6 mPa s by mixing glycerol and water to ensure that Taylor instabilities are absent in the Couette flow. Furthermore, the setup is restricted to low shear rates (1/s or 5/s) in order to avoid large gradients in the shear rate of the interface.

Image preparation

The shear cell was placed on the specimen table of an inverted microscope (Zeiss Axiovert 100). The microscope was equipped with long working-distance optics to view the air-liquid interface through the liquid medium. An objective of 32× or 20× lateral magnification was used with ordinary light transmission microscopy. For viewing a larger area, an objective of 8× lateral magnification was used with dark field microscopy. The magnified images were projected onto the CCD-chip of a 1/3″ CCD-camera (Hamamatsu C5405–10) capturing images of the aggregates. The video signal from the CCD-camera was contrast enhanced by a preprocessor (Hamamatsu Argus-20) before the images were digitised using a SLIC frame-grabber (MultiMedia Access Corporation) and stored on a Sun Ultra 1, UNIX work station. As a reference, the images were also video recorded (on a Sony SVO 9500 MDP). In this setup, the use of a 32× objective results in an effective image of 620×512 pixels, corresponding to an area of 156×129 μm (1 pixel = 0.252 μm).

Image analysis

The images were processed and analysed using an image analysis software (microGOP 2000S, Contextvision) to extract kinetic and structure information independently [8]. The kinetics may be described by dynamic scaling of the cluster-size distribution, n(s, t) [19]. This has previously been done for monodisperse systems [8]. In this work, images are analysed by a texture operation which, for the polydisperse emulsion system, results in a distribution of objects that correspond to the bright centres of the images of the drops. The objects are mathematically enlarged and overlapping objects are identified as part of a cluster. The enlargement of the objects depended on their individual sizes and was calibrated to connect the objects of a known large cluster. Once objects are identified as

being connected, the number of objects in the cluster is counted and the number included in the cluster-size distribution.

However, with the experimental setup in this work, drops of the smallest sizes are not resolved by the combination of the microscope and CCD-camera and the numbers of the smallest drop sizes are thus underestimated. Furthermore, determination of the full cluster-size distribution is precluded by the difficulty to distinguish between drops being at close separation and drops actually forming a bond. Hence, in this study, the analysis is limited to the basic aggregation processes for larger drops and clusters.

The structure is analysed by means of auto-correlation of large clusters spanning the whole image. The results from several images are averaged to yield the density auto-correlation function of the aggregate structure [20].

Results and discussion

Characteristics of the interfacial emulsion

We assume that the geometry of emulsion drops at the interface may be approximated by two segments of a sphere, one immersed in the aqueous phase and one extending into the vapour phase, see Fig. 1. The drop shape may be described by the angles of the spherical segments, θ_{aq} and θ_v, and the radius of the interfacial drop, a. These three parameters may be calculated from the interfacial energies, based on two assumptions: (i) the volume of the drops do not change when transferred to the air-liquid interface; (ii) mechanical equilibrium is established at the three-phase line. The latter results in relations for the angles of the segments of spheres:

$$\cos\theta_v = \frac{\gamma_{aqv}}{\gamma_{ov}} - \frac{\gamma_{aqo}^2 + \gamma_{aqv}^2 + \gamma_{ov}^2}{2\gamma_{ov}^2} \quad (1)$$

and

$$\cos\theta_{aq} = \frac{\gamma_{aqo}^2 + \gamma_{aqv}^2 - \gamma_{ov}^2}{2\gamma_{ov}\gamma_{aqo}} \quad (2)$$

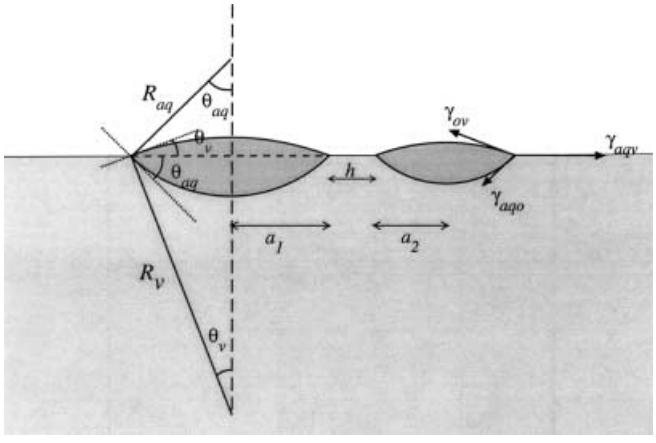

Fig. 1 Illustration of the drop geometry including different variables

where γ_{aqv} is the surface energy at the aqueous-vapour interface, γ_{ov} is the surface energy at the oil-vapour interface, and γ_{aqo} is the surface energy at the aqueous-oil interface. The volume of a spherical segment is a function of the angle θ and the interfacial drop radius a. Hence from the assumption of constant volume (i), we may relate the radius of the interfacial drop, a, with the radius of the drop in bulk, r, as $a = Qr$.

Interfacial energies relevant to the experimental conditions have been estimated by the pendant drop method for the aqueous-vapour interface, γ_{aqv}, as well as for the oil-vapour interface, γ_{ov}, and for the aqueous-oil interface, γ_{aqo}, Table 1. The results agrees fairly well with the work of Semenova et al. [18], which found an oil-water interfacial energy $\gamma_{ow} = 11$ mN/m^2 at a pectin concentration of 0.1%. In our measurements the aqueous phase consisted of 50/50% glycerol/water mixture including 0.008 wt% pectin, 0.3 mol/l $CaCl_2$, buffered to a pH of 8.4. The concentration of 0.008 wt% of pectin is well in excess of the bulk concentration calculated by assuming homogeneous mixing of the excess pectin in the continuous phase during aggregation experiments (i.e. 0.0005%). Inserting the measured interfacial energies into Eqs. (1) and (2) results in angles of the spherical sectors, given in Table 1, and a value of Q of 1.55.

The droplet geometry may also be affected by deformations at contact. The importance of such deformations can be estimated from the capillary number Ca:

$$Ca = \eta_o \dot{\gamma} a / \gamma_{aqo} \quad (3)$$

where η_o is the viscosity of the surrounding liquid and $\dot{\gamma}$ is the shear rate. For $\eta_o = 6$ mPa s, $\dot{\gamma} = 1$ s^{-1}, $\gamma_{aqo} = 13$ mN/m and $a = 1$ μm; Ca becomes very low ($Ca = 4.6 \times 10^{-7}$), suggesting that droplet deformations are negligible under the experimental conditions in this work. Hence, the dispersion interaction between two drops may be approximated by summation of the van der Waals interaction between the two pairs of spherical sectors, one pair in the vapour phase and one in the aqueous phase, as outlined for solid particles by Levine et al. [21]. The derivation is based on the Derjaguin approximation and results in the following relation:

Table 1 Interfacial energies and angles of segments of spheres at pH = 8.4

	0.008 wt% pectin, 0.3 mol/l $CaCl_2$ in glycerol/water
Interfacial energies	γ_{ov} = 29.2 γ_{aqo} = 13.6 γ_{aqv} = 35.0
Angles of segment of spheres	θ_{aq} = 50.5° θ_v = 32.6°

$$V_s(h) = -\frac{A_{aq}R_{aq}}{24h}\left(1 - \frac{L_{aq}}{\left(hR_{aq} + L_{aq}^2\right)^{1/2}}\right) - \frac{A_v R_v}{24h}\left(1 - \frac{L_v}{\left(hR_v + L_v^2\right)^{1/2}}\right) \quad (4)$$

where A_{aq} and A_v are the effective Hamaker constants for indentical phases and the indices aq and v denote intermediate medium of aqueous phase or vapour phase respective. Furthermore, h is the separation between the spherical segments of the interfacial droplets. In line with Fig. 1 with i = aq or v, we have $R_i = a/\sin\theta_i$, and $L_i = a/\tan\theta_i$ with which R_i and L_i is substituted to obtain the van der Waals contribution. From Eq. (4), with $A_{aq} = 3 \times 10^{-21}$ J and $A_v = 4 \times 10^{-20}$ J, values of $-9 \times 10^{-20} \le V_s \le -2.5 \times 10^{-20}$ J was obtained for the van der Waals interaction at separation distances between 1 nm and 10 nm.

The interfacial emulsion is stabilised against aggregation by short-range steric repulsion and long-range electrostatic repulsion due to adsorbed pectin at the aqueous-oil interface. The carboxyl groups in the pectin are ionised at the investigated pH (pH = 8.4) and we assume that these groups are preferentially oriented towards the aqueous phase. An attempt to measure the surface potential was made by electrokinetic measurements. Two sets of measurements were performed with the emulsion: in a glycerol/water mixture (50/50 w/w) and in Milli-Q water. Both systems contained 0.01 mol/l $CaCl_2$ and were buffered with 50 mmol/l TRIS to pH = 8.4. The emulsion displayed a ζ-potential, $\Phi \approx -13$ mV in water and $\Phi \approx -11$ mV in the aqueous mixture containing glycerol.

For a bulk system having such a low surface potential at high electrolyte concentration, the electrostatic repulsion becomes very short range and double-layer repulsion is not expected to stabilise the emulsion droplets. However, it is likely that the screening of surface charge is not as efficient at an air-liquid interface as in the bulk. Previous studies have shown that for charged latex particles, as much as 100 times more electrolyte is needed to aggregate an interfacial system, compared to a bulk system [2, 8, 20]. Consequently it is likely that also our interfacial emulsion system at least partly is stabilised by electrostatic repulsion.

In order to induce aggregation $CaCl_2$ was added to the system. High concentrations of Ca^{2+} will screen the electrostatic repulsion and may also induce bridging between the carboxylic groups on the adsorbed pectin.

Aggregation kinetics

The aggregation process by which clusters grow may be divided into heterogeneous or homogeneous cluster aggregation, i.e. addition of single particles or clusters to the growing clusters. During heterogeneous cluster aggregation, the number-average cluster size, N(t), and the weight-average cluster size, S(t), scale similarly with time. However, at homogeneous cluster aggregation S(t) increases more rapidly than N(t) with time. It was previously found that a transition between the two processes can occur, which depends on the magnitude of the attractive forces and the dominant transport mechanisms in the system. Such a transition of the dominating aggregation process may be identified by the polydispersity, P(t), of the cluster-size distribution [8, 22], defined as the ratio between the weight-average and the number-average cluster size.

Figure 2 shows the effect of salt concentration on the aggregation rate. Without salt, no formation of large clusters occurred but the polydispersity is not unity as particles are orbiting sufficiently close to each other to be interpreted in the image analysis as dimers and occasionally trimers. Increasing salt concentration results in a transition from constant to increasing polydispersity, which suggests that above the transition point aggregates grow by cluster-cluster aggregation rather than particle-cluster aggregation.

A system aggregating under shear displays a characteristic time scale, t_c, which is expected to scale according to

$$t_c = C\frac{W}{\phi\dot{\gamma}} \propto \frac{1}{\phi\dot{\gamma}} \quad . \quad (5)$$

where ϕ is the volume or area fraction of particles and the stability ratio, W, represents the inverse likelihood of bond formation at a collision. C is a numerical factor. At constant salt concentration, W is considered constant and ϕ and $\dot{\gamma}$ should determine the collision frequency

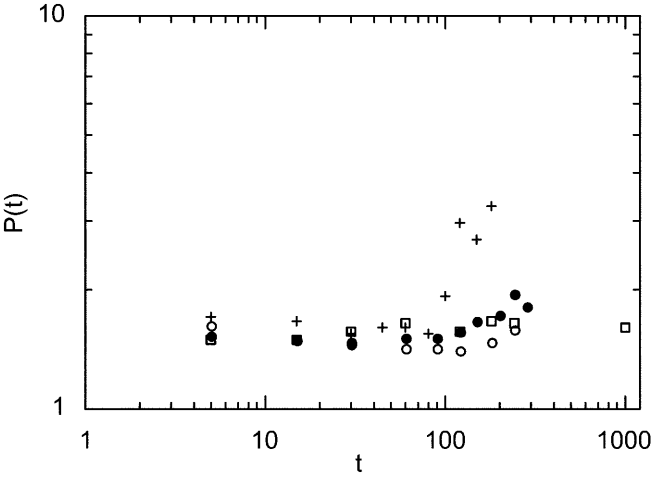

Fig. 2 Polydispersity, P(t), of the emulsion aggregates as function of time in minutes for $\phi \approx 0.1$ and $\dot{\gamma} = 1\ s^{-1}$ with different $CaCl_2$ concentrations: (□) 0.0 mol/l $CaCl_2$, (○) 0.1 mol/l $CaCl_2$, (●) 0.3 mol/l $CaCl_2$, (+) 0.5 mol/l $CaCl_2$

and t_c. However, we find that plotting in dimensionless form by putting $t^* = t/t_c = t\phi\dot{\gamma}$ does not collapse the data but indicates that aggregation is promoted if the area fraction of drops and the shear rate is reduced (Fig. 3). This seems inconsistent with the scaling above and we performed a simple dimension analysis in order to estimate other contributions to the characteristic time not accounted for in the simplified approach.

During initial heterogeneous aggregation, drops will stick or not stick depending on the strength of the interparticle attraction and the stress from the applied shear. This process may be regarded as a particle capture event where the polydispersity of the drop sizes is expected to be of importance. The efficiency of the capture event determines when a critical cluster size is reached and when homogeneous aggregation is expected to take over as the dominating aggregation process. A dimension analysis of the particle capture event [23] shows that both the Reynolds number and the Stokes number were low for our experimental conditions. Hence, inertial forces are unimportant. The relative motion between two particles results from convection and diffusion. The Péclet number expresses the ratio between the time scale for diffusion and convection and can be written as

$$\mathrm{Pe} = \frac{6\pi\eta_o a a_c^2\dot{\gamma}}{kT} \tag{6}$$

where η_o is the viscosity of the medium, a is the radius of the smaller particle, and a_c is the radius of the collector particle. At high Pe numbers, convection dominates and particles are restricted to follow the flow lines, whereas for low Pe numbers their relative motion is purely stochastic. Péclet numbers close to unity indicate that the trajectories vary randomly during the time scale of a collision. This may result in an enhancement of the aggregation rate if particle attractions are sufficiently long-range to create an asymmetry in the fluctuation of the trajectories. The attraction number, N_A,

$$N_A = \frac{A_{eff} a_c}{9\pi\eta_o a^4\dot{\gamma}} \tag{7}$$

expresses the ratio of the time scales for the passage and the time scale for the particle attraction to reduce the interparticle separation distance. This quantity also takes into account the lubrication forces, which tend to diminish the effect of the interparticle attraction.

We found that the Péclet number is in the order of unity for low shear rates ($\dot{\gamma} = 1\ s^{-1}$) and small drop sizes ($a = 0.1$ and $a_c = 1\ \mu m$). Furthermore, when the drop radius is a $\approx 0.1\ \mu m$ we obtain N_A in the range of 30 to 3500 for a collector radius of $a_c = 0.1$–$10\ \mu m$ and effective Hamaker constant $A_{eff} \approx 6 \times 10^{-21}$ J. The estimated values for Pe and N_A indicate that the aggregation rate may be enhanced by Brownian motion for large drop size differences. When the viscosity and the shear rate are increased, the influence of Brownian enhancement to the aggregation rate is expected to decrease. We incorporate the contribution of Brownian motion on the stability ratio and the aggregation rate by including N_A in a modified expression for the characteristic time:

$$t_c = C\frac{W}{N_A\phi\dot{\gamma}} = \frac{W\eta a^4\dot{\gamma}}{\phi\dot{\gamma}\ a_c A_{eff}} \propto \frac{\eta}{\phi}\ . \tag{8}$$

This suggests that the characteristic time should depend on the viscosity and the area fraction; the effect of shear rate is cancelled. We use the apparent viscosity, η, of the system instead of the viscosity of the medium, η_o, in the

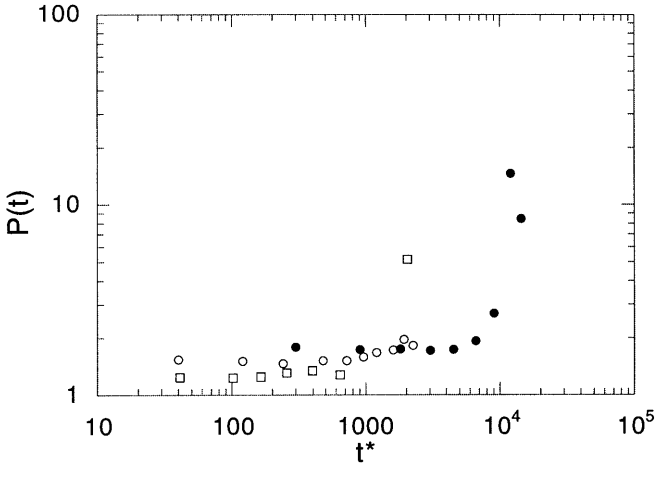

Fig. 3 Polydispersity, P(t), of the emulsion aggregates as function of dimension less time, $t^* = t\phi\dot{\gamma}$, for different area fraction of drops and shear rates at 0.3 mol/l $CaCl_2$: (□) $\phi \approx 0.03$ and $\dot{\gamma} = 1\ s^{-1}$, (●) $\phi \approx 0.2$ and $\dot{\gamma} = 5\ s^{-1}$, (○) $\phi \approx 0.12$ and $\dot{\gamma} = 1\ s^{-1}$

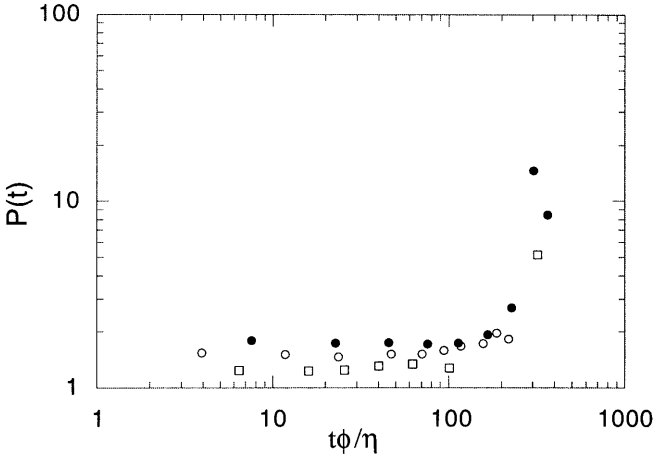

Fig. 4 Polydispersity, P(t), of the emulsion aggregates as function of reduced time, $t\phi/\eta$, for different area fraction of drops and shear rates at 0.3 mol/l $CaCl_2$: (□) $\phi \approx 0.03$ and $\dot{\gamma} = 1\ s^{-1}$, (●) $\phi \approx 0.2$ and $\dot{\gamma} = 5\ s^{-1}$, (○) $\phi \approx 0.12$ and $\dot{\gamma} = 1\ s^{-1}$

expression to account for hydrodynamic effects at higher drop concentrations. The apparent viscosity, η, is defined by $\eta_r\eta_o$ where η_o is the viscosity of the aqueous phase without emulsion (6 mPa s) and the relative viscosity η_r is obtained by a modified Krieger and Dougherty relation:

$$\eta_r = (1 - K\alpha\phi)^{-2.5/\kappa} \quad (9)$$

where the coefficient $K = 1.66$ and $\alpha \approx 0.94$ is a correction due to emulsion droplets not being solid; $\alpha = (\eta_i + 0.4\eta_o)/(\eta_i + \eta_o)$, where η_i is the viscosity of the oil [24]. From Eq (9), the following values for the relative viscosities were obtained: $\eta_r(\phi = 0.03) = 1.07$, $\eta_r(\phi = 0.12) = 1.32$, $\eta_r(\phi = 0.21) = 1.67$. Figure 4 shows the aggregation kinetics plotted as a function of the reduced time $t\phi/\eta$. The collapse of the data supports the conjecture that the characteristic time scale is proportional to the viscosity rather than the inverse shear rate. This is interesting since this is a similar scaling of t_c as for purely diffusion-controlled aggregation.

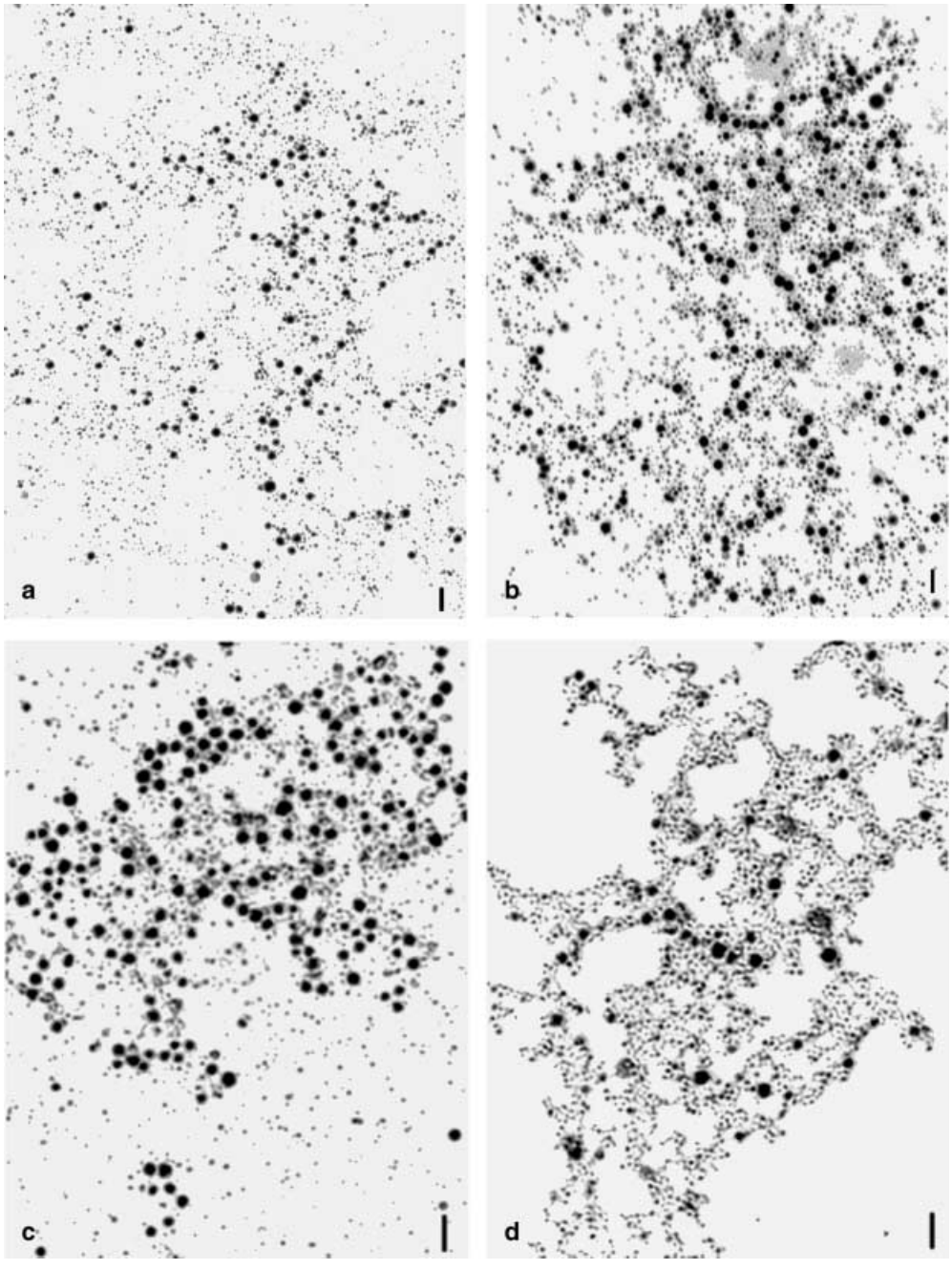

Fig. 5a–d Representative images of large clusters, which have been contrast enhanced and thresholded to improve printing. The length of the scale bars equals 10 μm **a** $\phi \approx 0.1$, $\dot{\gamma} = 1\ s^{-1}$ and 0.1 mol/l $CaCl_2$ after 999 min of shearing time (overnight); **b** $\phi \approx 0.1$, $\dot{\gamma} = 1\ s^{-1}$ and 0.5 mol/l $CaCl_2$ after 240 min shearing time; **c** $\phi \approx 0.2$, $\dot{\gamma} = 5\ s^{-1}$ and 0.3 mol/l $CaCl_2$ after 240 min shearing time; **d** $\phi \approx 0.03$, $\dot{\gamma} = 1\ s^{-1}$ and 0.3 mol/l $CaCl_2$ after 999 min shearing time

Structure

Large clusters, obtained at long aggregation times, were analysed for structural information. The representative raw data pictures of clusters in Fig. 5 exemplify the resulting structures at different conditions. In Fig. 5a, b (aggregated at a shear rate of 1/s with addition of 0.1 mol/l and 0.5 mol/l $CaCl_2$ respectively) we observe a similar, rather loose structure of fractal character with large and smaller drops distributed throughout the structures. Figure 5c, d represents changes in area fraction of drops and shear rate at a salt concentration of 0.3 mol/l $CaCl_2$. We find that the clusters in Fig. 5c ($\phi \approx 0.2$ and $\dot{\gamma} = 5\ s^{-1}$) display a more homogeneous pore size distribution compared with Fig. 5a, b. Furthermore, larger drops dominates more than in Fig. 5a, b. In Fig. 5d, where the area fraction was decreased to $\phi \approx 0.03$, we find a structure that consists of thicker strands with more medium-sized drops build up the structure compared to Fig. 5a, b.

The quantitative analysis of the structure of very large clusters was performed by auto-correlation of the cluster images. The reason for this is that even though the smallest drops are not properly resolved in the microscope, they still differ from the background and an enhanced image may be thresholded to infer their contribution to the structure. The slope of the linear part of the auto-correlation function (in a log-log plot, Fig. 6) is associated with the fractal dimension at that length scale [8, 20]. Changing the salt concentration did not change the fractal dimension ($d_f \approx 1.3$) but the density of the cluster was higher at a lower salt concentration. This implies that the structure and density of the basic building block differ and we have a more compact structure at small length scales with low salt concentrations. The slow aggregation rate and the low effective van der Waals attraction A_{eff} support a weakly bound structure. Hence, it is unexpected that the fractal dimension was as low as ≈1.3 as this value indicates an open structure which has not been rearranged by shear. One possible explanation is a contribution to the bond strength due to Ca^{2+} bridging between carboxylic groups of the pectin adsorbed to the oil-aqueous interface.

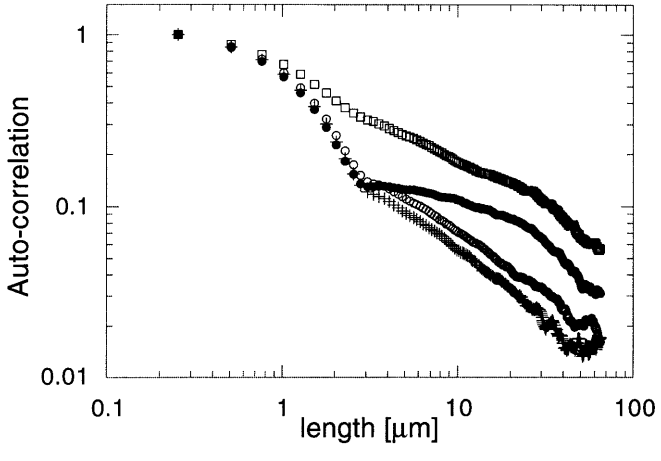

Fig. 6 Auto-correlation functions of large clusters for different systems: (○) $\phi \approx 0.1$, $\dot{\gamma} = 1\ s^{-1}$ and 0.1 mol/l $CaCl_2$, (+) $\phi \approx 0.1$, $\dot{\gamma} = 1\ s^{-1}$ and 0.5 mol/l $CaCl_2$, (□) $\phi \approx 0.03$, $\dot{\gamma} = 1\ s^{-1}$ and 0.3 mol/l $CaCl_2$, (●) $\phi \approx 0.2$, $\dot{\gamma} = 5\ s^{-1}$ and 0.3 mol/l $CaCl_2$

Decreasing the area fraction of drops has a profound effect on the structure. We do not observe a clear transition from the basic building block to the region of fractal scaling as for higher area fractions. The cluster density is much higher and the fractal dimension is increased as well, $d_f \approx 1.5$. Surprisingly, when both the area fraction and the shear rate was increased the fractal character disappears at the length scales accessible in the microscope. Hence, depending on the experimental conditions, the pectin stabilised emulsion displays clusters of fractal as well as non-fractal character. We speculate that this surprising feature may be due to a competition between possible combinations of drop sizes in the aggregation process. This competition results in cluster structures dominated by the most favourable drop size combination, determined by the experimental conditions (bond strength, shear rate and area fraction of drops) and the transport mechanisms.

Conclusion

We have used light microscopy and image analysis to study shear induced aggregation in two dimensions. The experimental system under study was a pectin-stabilised emulsion with drop sizes ranging between 0.1 μm and 40 μm in diameter. The basic aggregation mechanism was characterised by the polydispersity of the cluster size distribution and structural information was obtained by density auto-correlation analysis of large clusters.

The aggregation process was found to change from predominantly heterogeneous cluster aggregation to homogeneous cluster aggregation with time. However, the position of the transition point did not scale with the shear rate as expected for orthokinetic aggregation. Dimension analysis suggests that Brownian motion may increase the probability of the smaller drops to form bonds and participate in the cluster formation. Consequently, even though an increase in shear rate results in more collisions per unit time this does not increase the dimensionless aggregation rate because an increased shear rate also suppress the influence of Brownian motion. We found that a scaling of $t\phi/\eta$ was able to collapse the data on one master curve. This indicates that, even though convection is needed to aggregate the system, the characteristic time scales similarly to that of a diffusion-controlled system.

The cluster composition varied with the aggregating conditions. At low area fraction of drops and low shear rates, the structure consisted of a large fraction of small drops strongly rearranged at short length scales resulting in thick strands and a fractal dimensionality around 1.5. At higher area fractions of drops and higher shear rate, the clusters were dominated by the larger drops. This structure displayed no large pores and no fractal dimension could be determined for the accessible length scales. Finally, an increased salt concentration resulted in a less dense structure at the smallest length scale, probably due to increased bond strength between drops.

Acknowledgements This research was financed by the EU-FAIR project CT96-1216 and the Swedish National Board for Industrial and Technical Development (NUTEK). The authors would also like to thank the participants in the EU-FAIR project for fruitful discussions. Furthermore, we would like to thank Fresenius Kabi and the Institute for Research and Competence Holding AB (IRECO) for support in the development of the shear cell.

References

1. Poon WCK, Haw MD (1997) Adv Colloid Interface Sci 73:71
2. Hidalgo-Álvarez R, Martín A, Fernández A, Bastos D, Martínez F, de las Nieves FJ (1996) Adv Colloid Interface Sci 67:1
3. Hasmy A, Vacher R, Jullien R (1994) Phys Rev B 50:1305
4. Bushell G, Amal R (1998) J Colloid Interface Sci 205:459
5. Torres FE, Russel WB, Schowalter WR (1991) J Colloid Interface Sci 145:51
6. Torres FE, Russel WB, Schowalter WR (1991) J Colloid Interface Sci 142:554
7. Oles V (1992) J Colloid Interface Sci 154:351
8. Hansen PHF, Malmsten M, Bergenståhl B, Bergström L (1999) J Colloid Interface Sci 220:269
9. Axford SDT (1996) J Chem Soc Faraday Trans 92:1007
10. Wilson HJ, Pietraszewski LA, Davis RH (2000) J Colloid Interface Sci 221:87
11. Haw MD, Poon WCK, Pusey PN (1997) Phys Rev E 56:1918
12. Tokunaga K, Okuyama G, Nagasawa H, Otani Y (1981) Cosmet Toil 96:30
13. Mukerjee LN, Shukla SD (1971) Indian J Appl Chem 34:197
14. Graham DE, Phillips MC (1980) J Colloid Interface Sci 76:227
15. Graham DE, Phillips MC (1980) J Colloid Interface Sci 76:240
16. Dickinson E, Semenova MG, Antipova AS, Pelan EG (1998) Food Hydrocolloids 12:425–432
17. Murray BS, Færgemand M, Trotereau M, Ventura A (1999) In: Dickinson E, Rodrigues Patino JM (eds) Food emulsions and foams-interfaces, interactions and stability. Royal Society of Chemistry Special Publication 227, Cambridge, UK, pp 223–235
18. Semenova MG, Antipova AS, Belyakova LE, Dickinson E, Brown R, Pelan EG, Norton IT (1999) In: Dickinson E, Rodrigues Patino JM (eds) Food emulsions and foams-interfaces, interactions and stability. Royal Society of Chemistry Special Publication 227, Cambridge, UK, pp 163–175
19. Family F, Meakin P, Vicsek T (1985) J Chem Phys 83:4144
20. Robinson DJ, Earnshaw JC (1992) Phys Rev A 46:2045
21. Levine S, Bowen BD, Partridge SJ (1989) Colloids Surf 38:345
22. Hansen PHF, Bergström L (1999) J Colloid Interface Sci 218:77
23. Russel WB, Saville DA, Schowalter WR (1989) Colloidal dispersions. Cambridge University Press, pp 371–372
24. Dickinson E (1992) An introduction to food colloids. Oxford University Press